Infrared to Ultraviolet Measurements of Two-Photon Absorption and n_2 in Wide Bandgap Solids

Richard DeSalvo, *Member, IEEE*, Ali A. Said, David J. Hagan, *Member, IEEE*,
Eric W. Van Stryland, *Senior Member, IEEE*, and Mansoor Sheik-Bahae, *Member, IEEE*

Abstract—The bound electronic nonlinear refractive index, n_2, and two-photon absorption (2PA) coefficient, β, are measured in a variety of inorganic dielectric solids at the four harmonics of the Nd:YAG laser using Z scan. The specific materials studied are: barium fluoride (BaF$_2$), calcite (CaCO$_3$), potassium bromide (KBr), lithium fluoride (LiF), magnesium fluoride (MgF$_2$), sapphire (Al$_2$O$_3$), a tellurite glass (75%TeO$_2$+ 20%ZnO + 5%Na$_2$O) and fused silica (SiO$_2$). We also report n_2 and β in three second-order, $\chi^{(2)}$, nonlinear crystals: potassium titanyl phosphate (KTiOPO$_4$ or KTP), lithium niobate (LiNbO$_3$), and β-barium borate (β-BaB$_2$O$_4$ or BBO). Nonlinear absorption or refraction can alter the wavelength conversion efficiency in these materials. The results of this study are compared to a simple two-parabolic band model originally developed to describe zincblende semiconductors. This model gives the bandgap energy (E_g) scaling and spectrum of the change in absorption. The dispersion of n_2 as obtained from a Kramers–Kronig transformation of this absorption change scales as E_g^{-4}. The agreement of this theory to data for semiconductors was excellent. However, as could be expected, the agreement for these wide bandgap materials is not as good, although general trends such as increasing nonlinearity with decreasing bandgap energy can be seen.

I. INTRODUCTION

THE DISPERSION of the nonlinear refraction (NLR) and spectrum of nonlinear absorption (NLA) are measured in the following samples: barium fluoride (BaF$_2$), calcite (CaCO$_3$), potassium bromide (KBr), lithium fluoride (LiF), magnesium fluoride (MgF$_2$), sapphire (Al$_2$O$_3$), a tellurite glass (75%TeO$_2$+ 20%ZnO+ 5%Na$_2$O) and fused silica (SiO$_2$).[1] Measurements are made at the four harmonics of a TEM$_{00}$, single-pulse, picosecond Nd:YAG laser (i.e., $\lambda =$

[1]The cubic BaF$_2$ sample was supplied by Lawrence Livermore National Laboratory (LLNL) and is cut so that k is parallel to [100] and E parallel to [010]. The tetragonal MgF$_2$ sample was supplied by LLNL and has k parallel to [001] and E parallel to [100]. The cubic LiF$_2$ sample was supplied by LLNL and has unknown orientation. The trigonal Al$_2$O$_3$ and trigonal CaCO$_3$ samples have E parallel to a crystallographic axis. The KBr sample was obtained from Infrared Optical Products of New York.

1064 nm, 532 nm, 355 nm, and 266 nm). The spectral behavior of nonlinear effects in these inorganic solids is of interest because of their wide use as windows and elements in high-power laser systems. When these materials are used as passive elements in high-power laser systems, the intense optical fields change the optical properties of the material. These intensity-dependent changes in the material's optical properties affect the propagation of the incident light and govern the performance of the optical system. The refractive part of the nonlinearity gives rise to self-lensing, which can lead to catostrophic optical damage [1]–[3], and self-phase modulation is becoming increasingly important in the design of ultrafast laser systems. The absorptive part of the nonlinearity can decrease the transmittance at high irradiance and can provide a path for optical damage in the material at lower irradiances than conventional dielectric breakdown [3], [4].

In this study of transparent dielectrics, we are specifically interested in the ultrafast nonlinearities associated with two-photon absorption (2PA) and bound-electronic nonlinear refaction. The coefficients used for quantifying these processes are the 2PA coefficient, β, and the ultrafast nonlinear refractive index, n_2. The large bandgap energies of most of these materials allow measurement of n_2 and β from the near-infrared (1064 nm) to the ultraviolet (266 nm). These materials are assumed to become two-photon absorbing when the photon energy, $\hbar\omega$, equals one-half the bandgap energy, E_g. This occurs in several of these materials at the third or fourth Nd:YAG harmonic. The data collected here fills a relative void, as there are no previous studies where both NLA and NLR were measured over this large wavelength range.

Over the wavelength range studied, we do not observe the large dispersion including sign change as observed in smaller gap semiconductors [5]–[7]. A simple two-parabolic band model was very successful in predicting these nonlinearities in semiconductors [7], [8]. It predicts the nonlinear absorption spectrum and uses a Kramers–Kronig analysis to obtain n_2 [5]–[11]. The bandgap scaling and frequency dependence of n_2 and β were correctly described for semiconductors. While the agreement for semiconductors was remarkably good, the overall agreement for these wide bandgap materials is not as good. Here the data reasonably follows the predicted scaling for frequencies below the 2PA edge, however, for photon energies near or greater than the 2PA edge, the data quickly deviate from the predicted scaling of the two-band model. Moreover, we did not measure a negative n_2 for calcite at 266 nm as predicted by this model (also for BBO as discussed
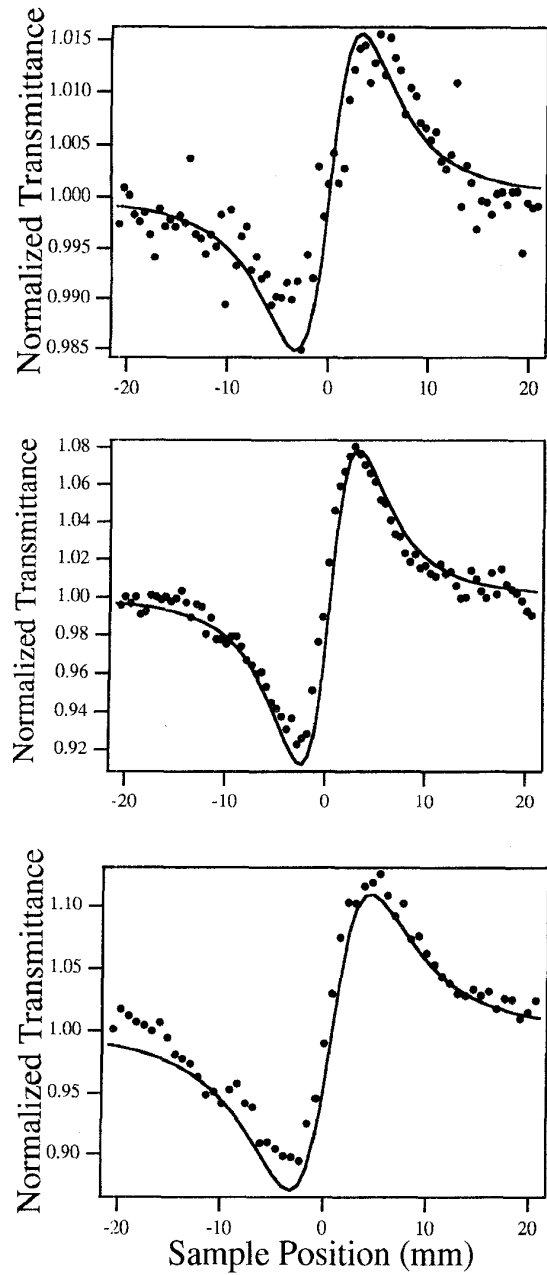
Fig. 1. Closed aperture Z-scans in single crystal BaF_2 showing a self-focusing nonlinearity at: a) 1064 nm, b) 532 nm, and c) 355 nm. Solid lines are fits.

Fig. 2. Z-scan traces in BaF_2 at 266 nm: (a) open aperture Z-scan showing 2PA, (b) closed aperture Z-scan showing both nonlinear refraction and 2PA, and (c) divided Z-scan showing a self-focusing nonlinearity. Solid lines are fits.

below). However, the bandgaps used for comparison are the linear transmission cutoff energies, which for dielectrics can be significantly below the direct energy gap due to indirect gap transitions, impurities, defects, and/or color center absorption. Using the measured 2PA spectrum to yield an effective direct-bandgap energy, E'_g, we find better agreement with the calculated values for n_2 in the ultraviolet.

We also report the dispersion of n_2 and spectrum of 2PA in three second-order nonlinear materials: potassium titanyl phosphate or KTP ($KTiOPO_4$), lithium niobate ($LiNbO_3$),
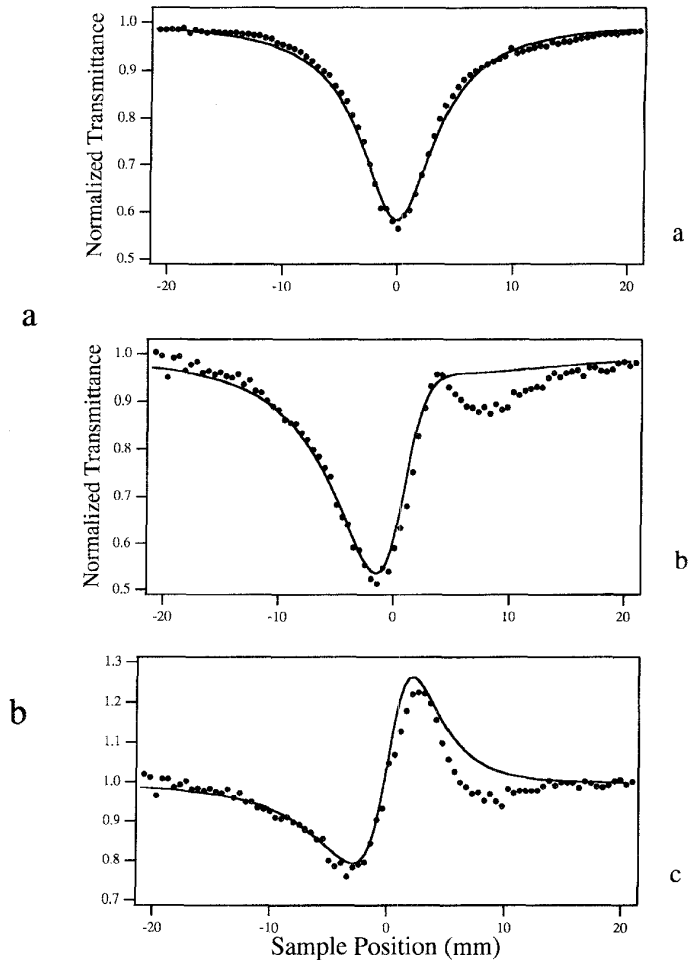
and β-barium borate or BBO (β-BaB_2O_4).[2] In these materials, NLA and NLR are of importance since either process can limit the frequency conversion efficiency (e.g., 2PA of the harmonic lowers the efficiency). Also, n_2 can alter the phase-matching conditions by changing the refractive index of the material in an anisotropic manner. While BBO's transmission range extends into the ultraviolet, allowing measurements at up to the third Nd:YAG harmonic, KTP and $LiNbO_3$ can only be measured up to the second harmonic due to residual linear losses at 355 nm.

II. MEASUREMENTS

We use the Z-scan [12] method that is described in detail in [13] to separately measure the NLA and NLR of these

TABLE I
SUMMARY OF THE EXPERIMENTALLY DETERMINED β AND n_2 ALONG WITH THE BANDGAP ENERGIES USED AS DISCUSSED IN THE TEXT

Material	E_g (eV)	E'_g (eV)	$n_2 \times 10^{-14}$ esu				β cm/GW		
			1064 nm	532 nm	355 nm	266 nm	532 nm	355 nm	266 nm
LiF	11.6	NM	2.5±0.5	1.9±0.4	1.9±0.4	4.0±1.0	≅ 0	≅ 0	≅ 0
MgF$_2$	11.3	NM	1.9±0.4	1.9±0.4	2.2±0.4	5.0±1.0	≅ 0	≅ 0	≅ 0
BaF$_2$	9.2	9.0	5.0±1.0	7.5±1.5	9.7±1.9	11±2	≅ 0	≅ 0	0.06±0.015
SiO$_2$	7.8	9.0	7.4±1.5	7.8±1.6	8.5±1.7	28±6	≅ 0	≅ 0	0.05±0.01
Al$_2$O$_3$	7.3	8.7	13±3	14±3	16±3	26±5	≅ 0	≅ 0	0.09±0.02
BBO	6.2	"6.8"	11±2	21±4	14±3	1±0.3	≅ 0	0.010±0.002	0.9±0.1
KBr	6.0	NM	29±6	47±9	NM	NM	≅ 0	NM	NM
CaCO$_3$	5.9	"8.0"	11±2	11±2	14±3	46±9	≅ 0	0.018±0.004	0.8±0.2
LiNbO$_3$	3.9	4.4	48±7	440±70	NM	NM	0.38±0.08	NM	NM
KTP	3.8	4.6	100±20	98±15	NM	NM	0.10±0.02	NM	NM
Te Glass	3.6	4.3	81±16	430±90	NM	NM	0.62±0.12	NM	NM

materials. The Z-scan is particularly useful for this spectral-dependence study since it is an absolutely calibrated method allowing measurements at different wavelengths to be compared. The sample thicknesses and irradiances used allow the "thin" sample approximation to be used, i.e., linear or nonlinear phase propagation effects within the sample are small [14].

The Q-switched and modelocked Nd:YAG laser used for these experiments produced TEM$_{0,0}$ mode, single 30-ps (FWHM) pulses (switched out) that were measured by a second-order autocorrelation technique [15]. To measure the frequency dependence of n_2 and β, we used nonlinear frequency conversion of the fundamental of Nd:YAG (1064 nm) to its harmonics (532 nm, 355 nm, and 266 nm) with KD*P crystals. Best-form focusing lenses ($f \simeq 150$ mm) were used for each of the four harmonic beams. The beam-waists, w_0 (HW1/e^2M), and pulsewidths, τ_p (FWHM), of the fundamental beam and its harmonics are respectively: at 1064 nm, 35 μm and 30 ps; at 532 nm, 24 μm and 22 ps; at 355 nm, 19 μm and 17 ps; at 266 nm, 16 μm and 15 ps. All irradiances are quoted within the sample, i.e., $I_0 = (1 - R)I$, where R is the Fresnel reflection coefficient, and I is the external irradiance. The overall experimental uncertainty is approximately ±20%. The primary uncertainties originate from the determination of the irradiance distribution used in the experiment, i.e., beam waist, pulsewidth, and energy calibration. All the quoted energies are calibrated against a Laser Precision RJ-7620 energy meter using the RJP-735 pyroelectric detector head. Relative errors are reduced by using energy windows and pulsewidth windows with the data aquisition system. For example, the pulsewidth of each laser firing is monitored by measuring the ratio of the square of the energy in the fundamental to the energy in the second harmonic and only pulses where this ratio is maintained within the range of ±10% are accepted [16]. Narrow band interference filters (spike filters) are used on the detectors for

TABLE II
LINEAR INDEX OF REFRACTION USED FOR THE MATERIALS STUDIED AT THE WAVELENGTHS USED

Material	1064 nm	532 nm	355 nm	266 nm
LiF	1.3	1.3	1.3	1.3
MgF$_2$	1.4	1.4	1.4	1.4
BaF$_2$	1.47	1.49	1.5	1.5
SiO$_2$	1.48	1.48	1.48	1.5
Al$_2$O$_3$	1.76	1.78	1.8	1.82
BBO	1.6	1.61	1.64	1.66
KBr	1.53	1.55		
CaCO$_3$	1.59	1.6	1.6	1.62
LiNbO$_3$	2.2	2.23		
KTP	1.77	1.78		
Te Glass	2.0	2.0		

each Z-scan measurement at a specific harmonic. This ensures the changes in transmittance monitored are not affected by flashlamp noise and other spurious light sources that may be present.

We show example data for BaF$_2$ in Figs. 1 and 2. The linear transmittance of BaF$_2$ cuts off at $\simeq 135$ nm. This corresponds to an optical gap of $E_g \simeq 9.2$ eV, therefore, BaF$_2$ should exhibit 2PA for photon energies $\hbar\omega$ such that 4.6 eV $< \hbar\omega <$ 9.2 eV. This corresponds to wavelengths <270 nm, which can be reached by the fourth-harmonic of Nd^{3+}:YAG at 266 nm. Closed aperture Z-scans (linear transmittance of the aperture $\simeq 40\%$) for BaF$_2$ at the fundamental, second harmonic, and third harmonic of the Nd^{3+}:YAG are shown in Fig. 1. No nonlinear absorption was observed at these wavelengths using open aperture Z-scans. For each of the Z-scan traces, we
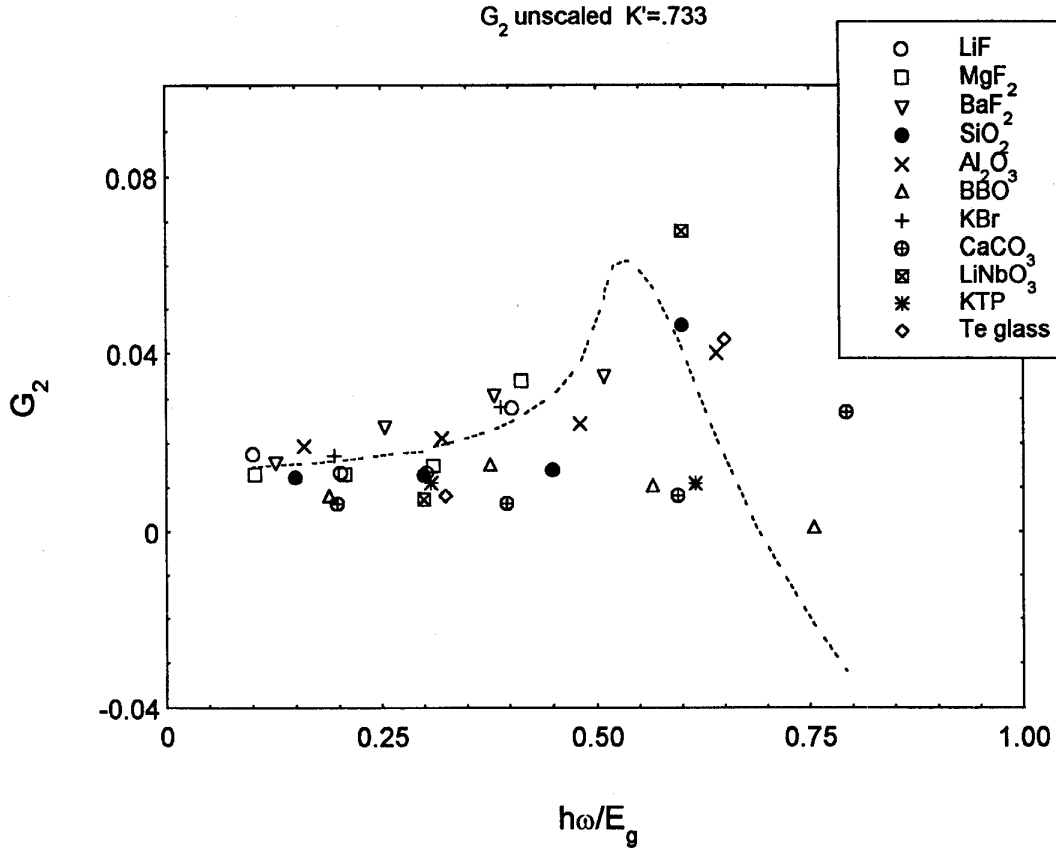
Fig. 3. Plot of the scaled n_2 data as a function of $\hbar\omega/E_g$, along with the theoretical dispersion function G_2 (solid line).

see a positive n_2. For example, using an irradiance $I_0 \simeq 103$ GW/cm^2 at 532 nm [Fig. 1(b)], a fit to the data gives $n_2 \simeq$ (2.1±0.4)× 10^{-16} cm/W or (7.5±1.5)× $10^{-14} esu$.

For an incident wavelength $\lambda = 266$ nm, which gives a photon energy of $\hbar\omega \simeq 4.7$ eV, 2PA is observed in BaF$_2$. Fig. 2(a) shows the open aperture Z-scan trace from which we determine a value of $\beta \simeq$ (0.06±0.015) cm/GW for $I_0 \simeq 72$ GW/cm^2 The closed aperture Z-scan is shown in Fig. 2(b). The fit gives a value of $n_2 \simeq$ (3.1 ± 0.6)× 10^{-16} cm^2/W or (1.1 ± 0.2)× $10^{-13} esu$. Dividing the data of Fig. 2(b) by the data of Fig. 2(a) gives data showing only the refractive part of the nonlinearity as plotted in Fig. 2(c) [13]. This figure shows the signature of a positive n_2. The dip in the data (deviation of the data from the fit) arises from surface irregularities or bulk inhomogeneities and is independent of irradiance, i.e., is a linear background effect. This can normally be subtracted by performing a Z-scan at very low irradiance levels where the nonlinear signal is small [13]. Our detector was not sensitive enough at this wavelength to accurately subtract this background, and the subtraction was not performed.

The measured values of n_2 and β for the materials studied are summarized in Table I. Details of material orientations and suppliers are given in the footnotes. The orientation dependence (i.e., anisotropy) of the nonlinear coefficients is generally small, being less than ±25% and, thus, does not significantly affect our conclusions [8]–[10], [17].

In this paper we define the nonlinear index by $n = n_0 + n_2\langle E^2\rangle$, where $\langle\ \rangle$ denotes a time average and n_0 is the linear index. The relation between n_2 in esu and in m^2/W is given by, $n_2(\text{esu}) = (cn_0/40\pi)\, n_2(\text{MKS})$. The values of the linear indexes used are given in Table II.

III. MODELING

The predicted scaling relation for the degenerate 2PA coefficient as calculated from second-order perturbation theory is given by [18], [19]

$$\beta(\omega) = \frac{K\sqrt{E_p}}{n_0^2 E_g^3} F_2(\hbar\omega/E_g).$$ (1)

The function F_2 depends on which states are optically coupled and gives the spectrum of degenerate 2PA. This function contains all the band structure related information in (1), and for the simplest possible case of two-parabolic bands is given by [6], [18], [19]

$$F_2(x) = \frac{(2x - 1)^{3/2}}{(2x)^5}.$$ (2)

The Kane momentum parameter, E_p, has a value near 21 eV for a number of materials [20]. It has not been measured for the materials we study here, and we assume it has this same value of 21 eV. Fitting the semiconductor data of [19] results in a best fit for the value of $K \simeq 3100$, where β is in
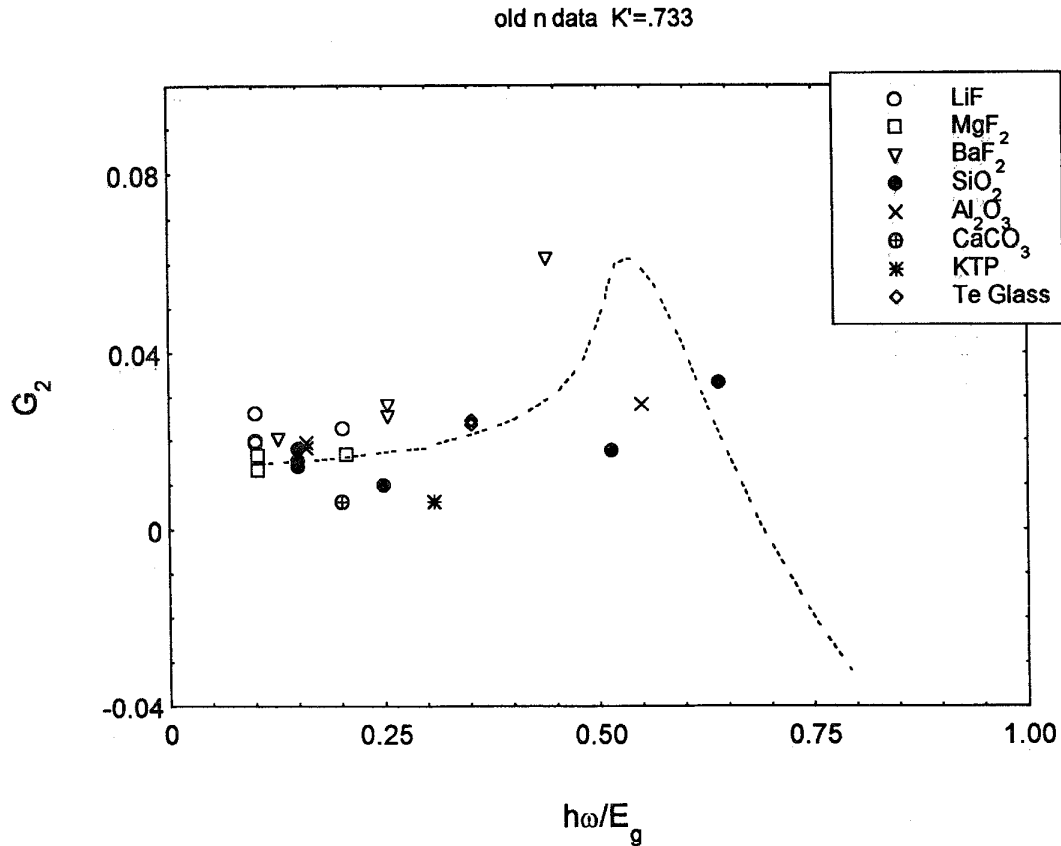
old n data K'=.733

Fig. 4.   Plot of scaled n_2 data from previous measurements along with G_2 (solid line). Data obtained from [21].

cm/GW and E_p and E_g are in eV. We use this value to scale the experimental 2PA data.

As shown in [5]–[7], [11], the nonlinear refactive index is given by a nonlinear Kramers–Kronig integral of the *nondegenerate* nonlinear absorption spectrum. The scaling relation for the degenerate n_2 is then given by

$$n_2(\text{esu}) = \frac{K'\sqrt{E_p}}{n_0 E_g^4} G_2(\hbar\omega/E_g) \qquad (3)$$

where the function G_2 contains the band-structure-dependent information, and the constant K' is directly related to the value of K. With E_p and E_g in eV, a value of $K = 3100$ gives a value of $K' = 7.33 \times 10^{-9}$ which is the value used throughout this paper. In [6], a value two times larger, $K' = 1.5 \times 10^{-8}$, was given. There, the factor of two difference between degenerate and nondegenerate index changes was not properly accounted for (see [9] for corrections).

In general, the Kramers–Kronig integral relates the nondegenerate NLR to the nondegenerate NLA and vice-versa. Here we give the relation for the degenerate $n_2(\omega_2)$ in terms of an integral over all frequencies, ω_1, of the absorption change due to a fixed input at energy $\hbar\omega_2$. The dispersion function G_2 is then given by

$$G_2(x_2) = \frac{2}{\pi} \int_0^\infty \frac{F_2(x_1; x_2)}{x_1^2 - x_2^2} \, dx_1 \qquad (4)$$

where $F_2(x_1; x_2)$ gives the nondegenerate nonlinear absorption spectral dependence and $x_i = \hbar\omega_i/E_g$ [6].

While the functional dependence of the degenerate 2PA coefficient is relatively simple within the two-parabolic band model, i.e., $F_2(x)$, the corresponding dependence of the *nondegenerate* 2PA and, in turn, n_2 is complex [6], [9], [10]. This is further complicated by the fact that NLR depends upon all nondegenerate nonlinear absorption processes including electronic Raman and AC–Stark contributions, which must be included in $F_2(x_1; x_2)$. The specific functional dependencies are given in [6] for the two-parabolic band model (see [9] for corrections). There, the expected E_g^{-4} scaling in (3) is seen as predicted by Wherrett [18].

Fig. 3 shows our measured values obtained for n_2 scaled by $n_0 E_g^4 / K'\sqrt{E_p}$ versus $\hbar\omega/E_g$. From (3), this gives an experimental equivalent of the dispersion function G_2 which is also included on the same graph for comparison. Previous n_2 measurements for these materials are shown with the same scaling in Fig. 4 [21].

As seen in Fig. 3, data agree with the calculation for $\hbar\omega$ below the 2PA edge ($\hbar\omega = 0.5$) within approximately a factor of two. For example, LiF and MgF_2 possess the largest band gaps ($\simeq 11$ eV) of the materials studied. Here, we see relatively good agreement with the scaling predicted by the two-parabolic band model even for the 355-nm and 266-nm data. MgF_2 is a tetragonal crystal and has an indirect gap.
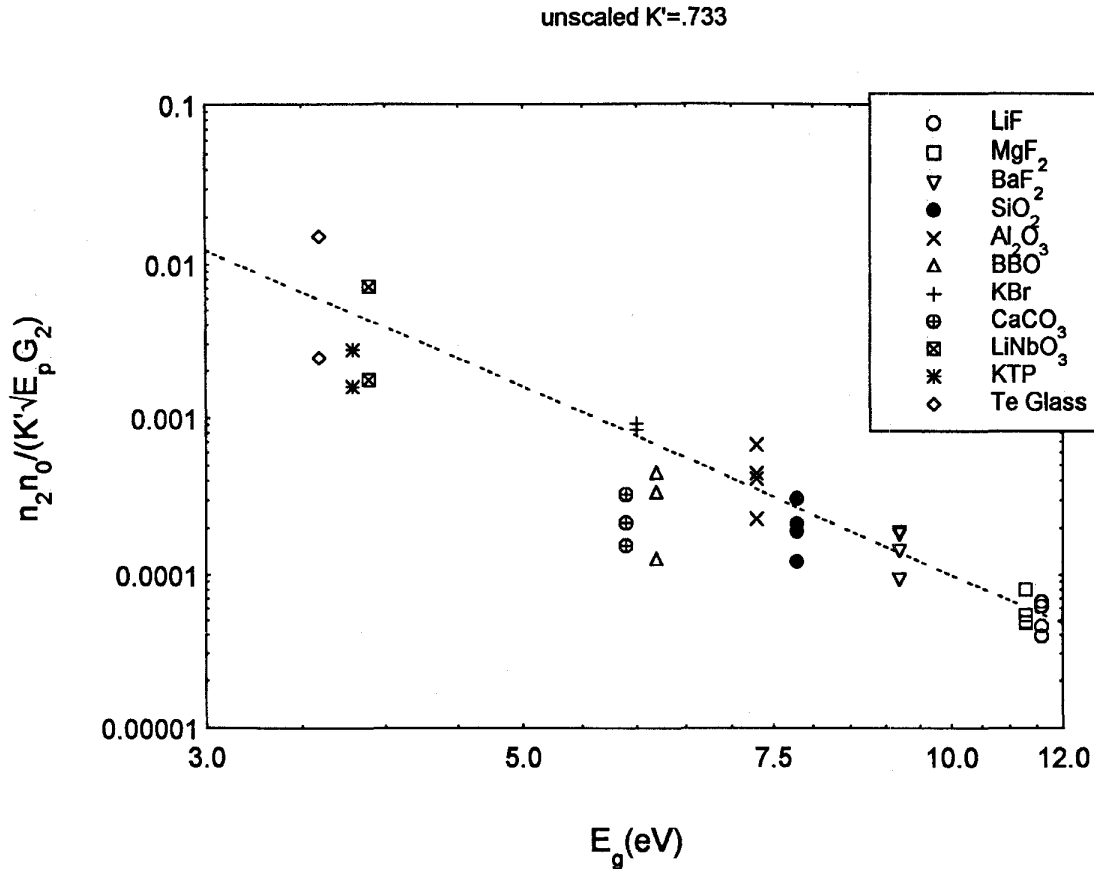
Fig. 5.   4. A log-log plot of the scaled n_2 data of Fig. 3 versus E_g, showing the predicted E_g^{-4} dependence (solid line).

The data for MgF_2 follows the scaling but, being somewhat smaller, does not agree in absolute magnitude as well as data for BaF_2 or LiF which are cubic direct-gap crystals [22]. For materials with smaller bandgap energies, the experimental data appear to diverge from the prediction of the two-parabolic band model when the incident photon energy is near the 2PA edge. In addition, we did not see the predicted negative n_2 values for calcite or BBO at 266 nm.

Hidden in Fig. 3 is the several orders-of-magnitude variation of n_2 due to the E_g^{-4} scaling. This variation is better shown on the log-log plot of Fig. 5. This figure shows n_2 data multiplied by n_0 and divided by the theoretical dispersion function G_2 as a function of E_g. Theory predicts that both graphs (Figs. 3 and 5) are universal curves, independent of material. Thus, in Fig. 5, data at different wavelengths for a single material should all lie on top of one another. Note, a datum for BBO at 266 nm which gave a very small but positive n_2 is not shown as it lies well below the bottom of the graph.

It is interesting to examine the spectrum of the experimental 2PA data. Fig. 6 is a plot of this data scaled by $n_0^2 E_g^3 \sqrt{E_p K}$ (i.e. the experimental F_2) as a function of $\hbar\omega/E_g$. It is apparent from Fig. 6(a) that the theory consistently overestimates β. This would be possible if the 2PA edges of the materials plotted were underestimated. We calculate the 2PA edge as $E_g/2$ where E_g is determined from the linear transmittance cutoff frequency, i.e., the ultraviolet optical absorption edge.

If we assume that this observed absorption onset is due to impurity levels [23], indirect gap transitions, defects, or self-trapped excitons [24], the direct gap could be significantly higher than the linear absorption cutoff energy.

If we allow the direct gap energy E_g to vary, so as to make β fit (1), we obtain a new effective bandgap energy, $E_g' = \zeta E_g$. For the materials studied where 2PA is observed, this results in an increase in $E_g (\zeta > 1)$ except for BaF_2 which is shifted $\simeq 2\%$ downward, a negligible change. When we make a shift of the x axis by ζ in Fig. 6(a), we must make a shift of the y axis by ζ^3. We rescale data for fused silica (266 nm), sapphire (266 nm), BBO (355 and 266 nm), calcite (355 nm and 266 nm), $LiNbO_3$ (532 nm), KTP (532 nm), and tellurite glass (532 nm). For materials where two values of β were obtained, an average ζ was determined.

We now use the newly assigned bandgap energies E_g' to recalculate n_2. This results in somewhat better agreement with (3), however, there is still a sign discrepancy for BBO at 266 nm, and the experimental n_2 at 266 nm for calcite is 23 times larger than predicted. If the bandgap for BBO is further increased from 6.45 eV to 6.8 eV (a 5% increase), the n_2 datum at 266 nm can be made to agree with (3) and (4). This only leads to a small discrepancy with the β values at 266 nm ($\beta = 0.77$ cm/GW rather than the experimentally observed 0.9 cm/GW) and at 355 nm ($\beta = 0.066$ cm/GW rather than the experimentally observed 0.01 cm/GW). This shift eliminates
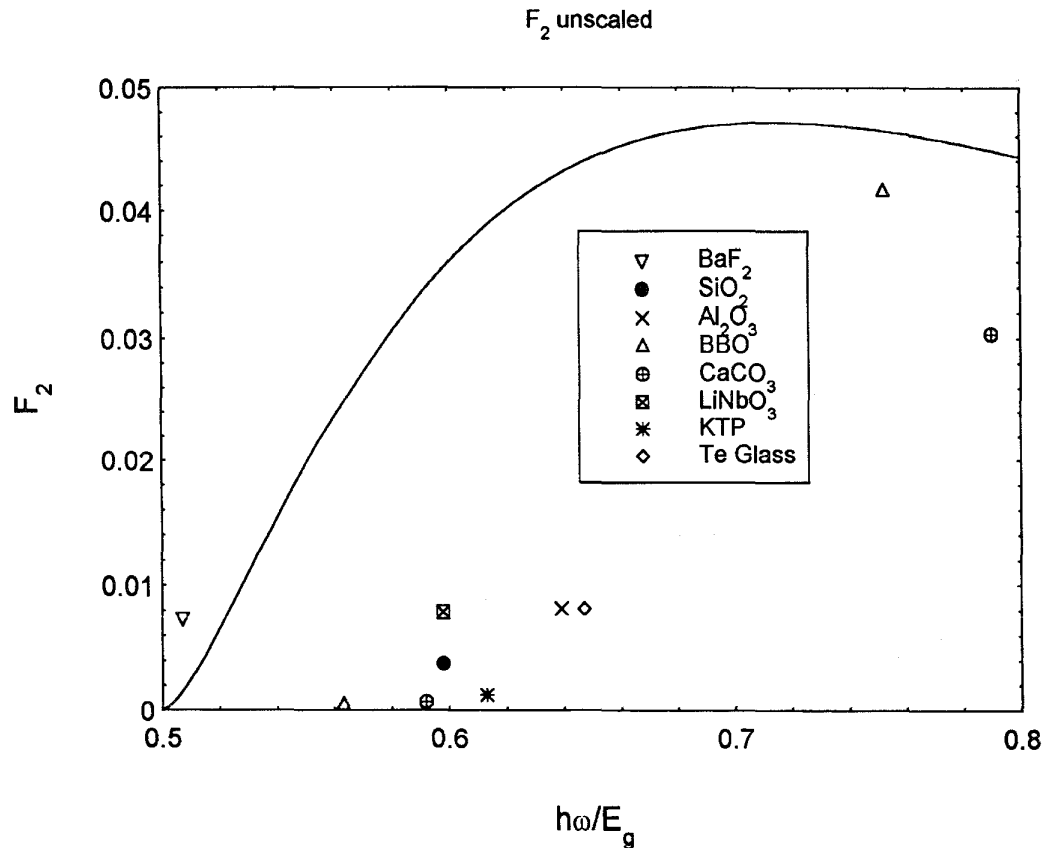
Fig. 6. Spectrum of the scaled experimental values of β. The solid line shows the prediction of the two-parabolic band model.

the discrepancy in sign for n_2 at 266 nm but the resulting value for n_2 at 355 nm does not show an enhancement around the new 2PA edge (which now lies near 355 nm).

The discrepancies for $CaCO_3$ are even more significant. Shifting E_g to $E'_g \simeq 6.8$ eV (a 15% increase) gives excellent agreement for the β values at both 266 nm and 355 nm, however, the experimental value of n_2 at 266 nm is 23 times larger than predicted. In order for calcite data to match the predicted dispersion, a value of $E'_g \simeq 8$ eV is needed (a further increase of 16%). This would also place the 355-nm datum below the 2PA edge where β should vanish. However, the very small value of β at 355 nm of 0.018 cm/GW is consistent with indirect gap 2PA. For this value of β to be due to direct gap 2PA would require 355 nm to lie very close to the 2PA edge (note that this is also true for BBO at 355 nm where the small experimental value of β is consistent with indirect gap 2PA). If we assume that calcite is an indirect gap material and that $E'_g \simeq 8$ eV, the n_2 data closely follow the predicted scaling relations and the value of β at 266 nm is predicted to be 0.33 cm/GW as opposed to the experimental value of 0.8 cm/GW, i.e., within expectations.

Fig. 7 shows the results of rescaling the data using E'_g, plotted with the predicted dispersion curve, G_2. The values used for E'_g are listed in Table I (the values for BBO of 6.8 eV and for calcite of 8 eV were used). The data of Fig. 3 are shifted up and to the left by this increase in bandgap energy.

We now obtain better agreement for n_2 with the two-parabolic band calculation around the 2PA edge where some data show the predicted enhancement, whereas in Fig. 3, the scaled data remain relatively constant throughout the measured spectrum. The largest disparity is for BBO at 355 nm which is a factor of 4.5 lower than the theory. Most data falls within a factor of two of the prediction. Fig. 8 shows a log-log plot for the rescaled data where we now find much of the data straddling either side of the predicted E_g^{-4} line (all data now lie on the graph).

Rescaling the bandgap energy in accordance with 2PA measurements has precedence. Fröhlich and Staginnus [25] have previously shown bandgap reassignment in alkali bromides by using two-photon spectroscopy. Bosio and Czaja [26] found that using a bandgap energy of 9.1 eV fits their analysis of the Urbach edge [27] in amorphous silicon dioxide (αSiO_2). This is nearly identical to our E'_g of 9.0 eV found by shifting the 2PA data. Ching and Xu [28] calculated the band structure of KTP and obtained a direct gap of $\simeq 4.9$ eV, which is close to our E'_g of $\simeq 4.6$ eV. Sapphire, although an indirect gap material, may be approximated as a direct gap insulator as the energy difference between indirect and direct gaps is small [29]. Measured experimental values of the bandgap in sapphire range from 8.7 eV to 9.4 eV [29]. Our value of $E'_g = 8.7$ eV is within this range. Little information on the bandgap of BBO exists, however, BBO and LiB_3O_5 (lithium triborate or LBO)
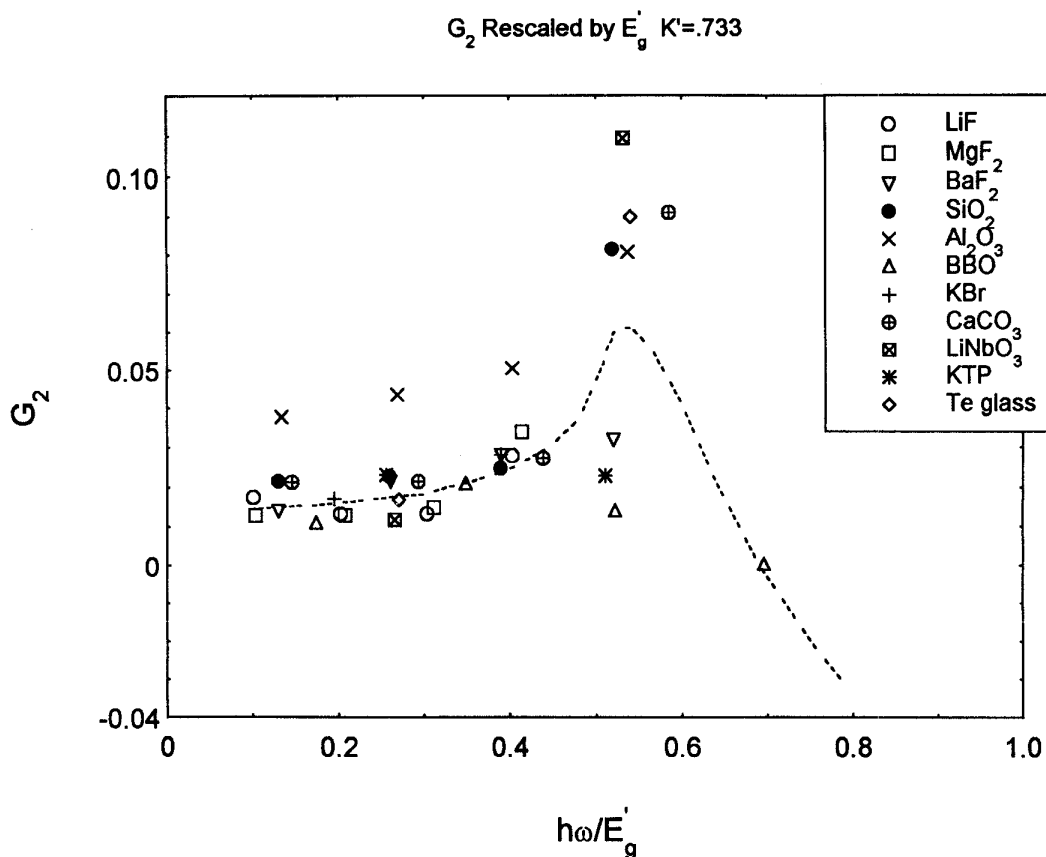
Fig. 7. Plot of the dispersion of n_2 rescaled with E'_g, as a function of $\hbar\omega/E'_g$.

have similiar linear optical properties, i.e., refractive index and transmittance window. The electronic structure of LBO was calculated by Xu and Ching [30] from which a direct gap of 7.4 eV was found. Because of the structural and optical similiarities, our value of $E'_g \simeq 6.8$ eV for BBO appears to be reasonable.

IV. CONCLUSION

We have extended measurements of the bound-electronic nonlinear refractive index, n_2, and two-photon absorption coefficient, β, to wide bandgap dielectric materials to frequencies available from the harmonics of the Nd:YAG laser, i.e., 1064, 532, 355, and 266 nm. The purpose of this study was both to extend the database and to determine the validity of the very successful two-parabolic band model that predicts these nonlinearities in semiconductors [6], [7], [9], [19]. That theory, which predicts the nondegenerate (and degenerate) nonlinear absorption spectrum and used a Kramers–Kronig analysis to obtain the dispersion of n_2, gives the bandgap scaling and frequency dependence of n_2 and β correctly for a wide variety of materials. It also gives values of n_2 for wide bandgap materials to within a factor of 2 to 3 for frequencies far below the band edge. This study extends the frequency range of data much nearer to the band edge in these materials. One of the difficulties in determining the validity of the two-band model is that it is based on a single direct bandgap. In many of the

dielectric materials studied, this is a poor approximation for the linear behavior. What we determine is that if the bandgap is defined as the linear absorption cutoff energy, agreement is relatively poor, and even the sign of n_2 is incorrectly predicted for two of the materials studied at 266 nm. However, another method previously used to define the bandgap is the energy of the two-photon absorption edge. By forcing our measured values of β to fit the two-parabolic band model by allowing E_g to increase, better agreement is obtained for n_2 although significant discrepancies remain for BBO and calcite. A further increase in bandgap energy for BBO and calcite to reach a compromise agreement with theory for the n_2 and β data reduces these discrepancies. These new bandgaps (E'_g) can be considered effective direct gaps for each material. The bandgap energy values obtained are found to be consistent with previous studies. We also note that this procedure is incomplete in that we only have 2PA data for those materials with bandgap energy low enough to exhibit 2PA at 266 nm.

This two-parabolic band model is clearly an oversimplification and more sophisticated models are needed to give the details of the dispersion of n_2 and spectrum of β. For example, [31] showed the existence of an anisotropic 2PA coefficient can be explained by including the effects of higher bands, and measurements showed good agreement [32]. Clearly, anisotropy in β also leads to anisotropy in n_2. However, the overall agreement within factors of 2 or 3 for such a large
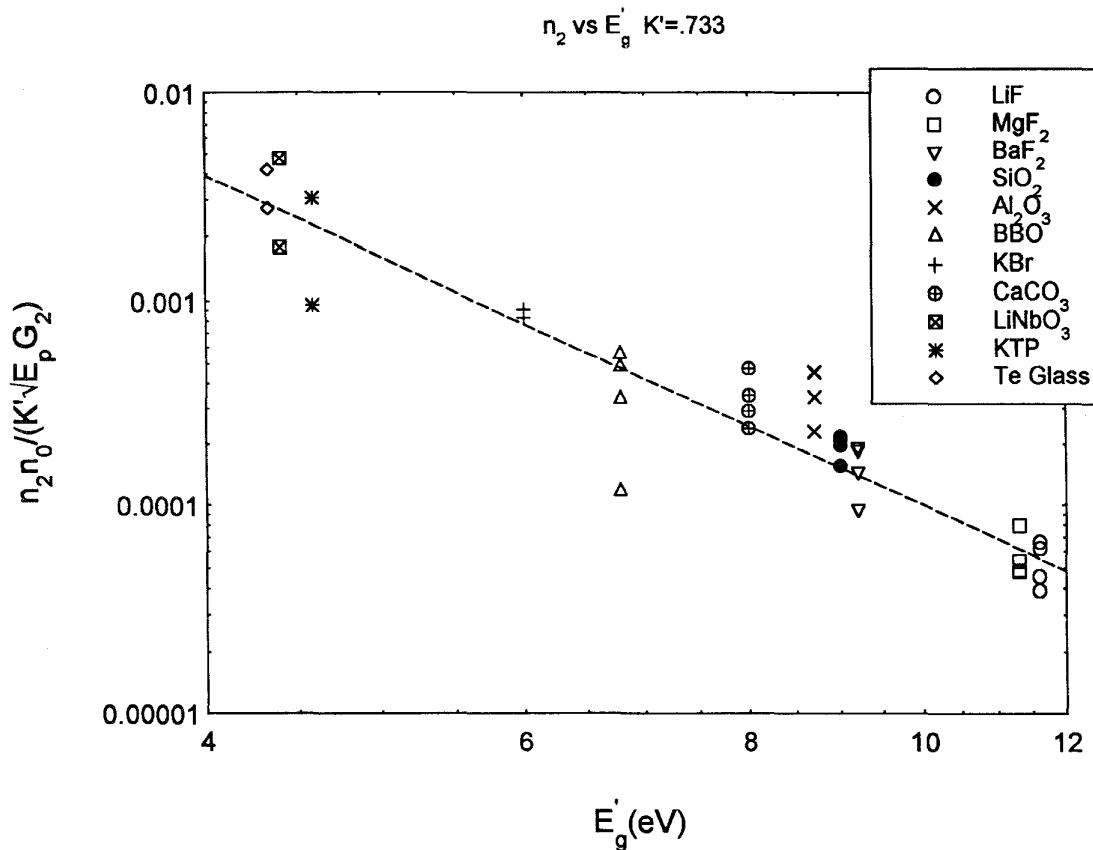
Fig. 8.   A log-log plot of the data rescaled with E'_g, as a function of E'_g.

class of materials over such a large frequency range (1064 nm to 266 nm) for a greater than 10^2 change in magnitude of n_2 shows that the basic physics of the interactions are being included here, and that the details of the band stucture, while playing a significant role, do not play the dominant role in determining these nonlinearities.

ACKNOWLEDGMENT

REFERENCES

[1] P. L. Kelly, "Self-focusing of optical beams," *Phys. Rev. Lett.,* vol. 15, pp. 1005–1008, 1965.
[2] W. L. Smith, J. H. Bechtel, and N. Bloembergen, "Dielectric-breakdown threshold and nonlinear-refractive-index measurements with picosecond laser pulses," *Phys. Rev. B,* vol. 12, pp. 706–714, 1975.
[3] M. J. Soileau, W. E. Williams, N. Mansour, and E. W. Van Stryland, "Laser-induced-damage and the role of self-focusing," *Opt. Eng.,* vol. 28, pp. 1133–1144, 1989.
[4] N. Mansour, K. Mansour, M. J. Soileau, and E. W. Van Stryland, "Observation of two-photon absorption prior to laser-induced damage

in ZrO_2," in *Laser Induced Damage in Optical Materials, NIST Special Publication,* vol. 756, p. 501, 1987.
[5] M. Sheik-Bahae, D. J. Hagan, and E. W. Van Stryland, "Dispersion and band-gap scaling of the electronic Kerr effect in solids associated with two photon absorption," *Phys. Rev. Lett.,* vol. 65, pp. 96–99, 1990.
[6] M. Sheik-Bahae, D. C. Hutchings, D. J. Hagan, and E. W. Van Stryland, "Dispersion of bound electronic nonlinear refraction in solids," *IEEE J. Quantum Electron.,* vol. 27, pp. 1296–1309, 1991.
[7] D. C. Hutchings, M. Sheik-Bahae, D. J. Hagan, and E. W. Van Stryland, "Kramers–Kronig relations in nonlinear optics," *Opt. Quantum Electron.,* vol. 24, pp. 1–30, 1992.
[8] M. Sheik-Bahae, J. Wang, R. DeSalvo, D. J. Hagan and E. W. Van Stryland, "Measurement of nondegenerate nonlinearities using a 2-color Z-scan," *Opt. Lett.,* vol. 17, pp. 258–260, 1992.
[9] M. Sheik-Bahae, J. Wang, and E. W. Van Stryland, "Nondegenerate optical Kerr effect in semiconductors," *IEEE J. Quantum Electron.,* vol. 30, pp. 249–255, 1994.
[10] D. C. Hutchings and E. W. Van Stryland, "Nondegenerate two-photon absorption in zinc blende semiconductors," *J. Opt. Soc. Amer. B,* vol. B9, pp. 2065–2074, 1992.
[11] F. Bassani and S. Scandolo, "Dispersion relations in nonlinear optics," *Phys. Rev.,* vol. B44, pp. 8446–8453, 1991.
[12] M. Sheik-Bahae, A. A. Said, and E. W. Van Stryland, "High sensitivity, single-beam n_2 measurements," *Opt. Lett.,* vol. 14, pp. 955–957, 1989.
[13] M. Sheik-Bahae, A. A. Said, T. H. Wei, D. J. Hagan, and E. W. Van Stryland, "Sensitive measurement of optical nonlinearities using a single beam," *IEEE J. Quantum Electron.,* vol. 26, pp. 760–769, 1990.
[14] A. E. Kaplan, "External self-focusing of ligth by a nonlinear layer," *Radiophys. Quantum Electron.,* vol. 12, pp. 692–696, 1969.
[15] J. A. Armstrong, "Measurement of picosecond laser pulse widths," *Appl. Phys. Lett.,* vol. 10, pp. 16–18, 1967.
[16] W. H. Glen and M. J. Brienza, "Time evolution of picosecond pulses," *Appl. Phys. Lett.,* vol. 10, pp. 221, 1967.
[17] R. DeSalvo, M. Sheik-Bahae, A. Said, D. Hagan, and E. Van Stryland, "Z-scan measurement of the anisotropy of nonlinear refraction and absorption in crystals," *Opt. Lett.,* vol. 18, pp. 194–196, 1993.

[18] B. S. Wherrett, "Scaling rules for multiphoton interand absorption in semiconductors," *J. Opt. Soc. Amer. B*, vol. 1, pp. 67–72, 1984.

[19] E. W. Van Stryland, H. Vanherzeele, M. A. Woodall, M. J. Soileau, A. L. Smirl, S. Guha, and T. F. Boggess, "Two photon absorption, nonlinear refraction and optical limiting in semiconductors," *Opt. Eng.*, vol. 24, pp. 613–623, 1985.

[20] E. O. Kane, "Band structure of indium antimonide," *J. Chem. Phys. Solids*, vol. 1, pp. 249–261, 1957.

[21] L .L. Chase and E. Van Stryland, "Nonlinear refractive index: inorganic materials," in *Handbook of Laser Science and Technology; Supplement 2: Optical Materials*, M. Weber, Ed. Boca Raton, FL: CRC Press, 1994, sect. 8, pp. 269–288.

[22] D. M. Drost and J. L. Fry, "A self-consistant procedure for the linear combination-of-atomic-orbitals method: Application to LiF," *Phys. Rev. B*, vol. 5, pp. 684–697, 1972.

[23] R. Blachman, Crystal Technology, private communication, 1993.

[24] N. Itoh and K. Tanimura, "Effects of photoexcitation of self trapped excitons in insulators," *Opt. Eng.*, vol. 28, pp. 1034–1038, 1989.

[25] D. Frohlich and B. Staginnus, "New assignment of the band gap in the alkalai bromides by two-photon spectroscopy," *Phys. Rev. Lett.*, vol. 19, pp. 496–498, 1967.

[26] C. Bosio and W. Czaja, "Urbach tails in the absorption spectra of amorphous and crystalline SiO_2," *Philos. Mag.*, vol. B63, pp. 7–14, 1991.

[27] F. Urbach, "The long-wavelength edge of photographic sensitivity and of the electronic absorption of solids," *Phys. Rev.*, vol. 92, p. 1324, 1953.

[28] W. Y. Ching and Y.-N. Xu, "Band structure linear optical properties of $KTiOPO_4$," *Phys. Rev. B*, vol. 44, pp. 5332–5335, 1991.

[29] Yong-Nian Xu and W. Y. Ching, "Self-consistant band structures, charge distributions, and optical-absorption spectra in MgO, α-Al_2O_3, and $MgAl_2O_3$," *Phys. Rev. B*, vol. 43, pp. 4461–4472, 1991.

[30] Y.-N. Xu and W. Y. Ching, "Electronic structure and optical properties of LiB_3O_5," *Phys. Rev. B*, vol. 41, pp. 5471–5474, 1990.

[31] D. C. Hutchings and B. S. Wherrett, "Theory of the anisotropy of two photon absorption in zinc-blende semiconductors," *Phys. Rev. B*, vol. 49, pp. 2418–2426, 1994.

[32] M. Dvorak, W. A. Schroeder, D. Anderson, A. L. Smirl, and B. S. Wherrett, "Measurement of the anisotropy of two-photon absorption coefficients in zincblende semiconductors," *IEEE J. Quantum Electron.*, vol. 30, pp. 256–268, 1994.

Richard DeSalvo (S'91–M'94), photograph and biography not available at the time of publication.

Ali A. Said, photograph and biography not available at the time of publication.

David J. Hagan (M'87), photograph and biography not available at the time of publication.

Eric W. Van Stryland (M'84–SM'90), photograph and biography not available at the time of publication.

Mansoor Sheik-Bahae (M'87), photograph and biography not available at the time of publication.